

Special Issue: Plant Bioactive from the Palms and other Horticultural Crops

Evaluation of particle size on the physicochemical properties of *Moringa oleifera* Lam. stem powder

Yue Zhang¹, Kehong Liang², Jing Wang², Aili Wang³, R. Pandiselvam⁴, and Hong Zhu^{2*}

¹College of Engineering, China Agricultural University, Beijing, China; ²Institute of Food and Nutrition Development, Ministry of Agriculture and Rural Affairs, Beijing, China; ³School of Food and Biological Engineering, Key Laboratory of Coarse Cereal Processing (Ministry of Agriculture and Rural Affairs), Chengdu University, Chengdu, China; ⁴Division of Physiology, Biochemistry and Post-Harvest Technology, ICAR-Central Plantation Crops Research Institute, Kasaragod, India

*Corresponding Author: Hong Zhu, Institute of Food and Nutrition Development, Ministry of Agriculture and Rural Affairs, No. 12 Zhongguancun South Street, Haidian District, Beijing 100081, China. Email: zhuhong@caas.cn

Received: 17 May 2022; Accepted: 23 June 2022; Published: 11 July 2022

© 2022 Codon Publications

OPEN ACCESS 

ORIGINAL ARTICLE

Abstract

Moringa oleifera Lam. stem (MOS) has been used for beneficial dietary and medicinal purposes. In this work, MOS samples of six different particle sizes were produced using sieve-based mechanical grinding to investigate the impact of varying particle sizes on the physicochemical properties of MOS powder. Scanning electron microscopic images revealed the destroyed fiber structures after grinding. The color turned greener and less yellow with decreasing particle size. The angle of repose significantly decreased from 70.36° to 60.25°, as the particle size declined, demonstrating the increasing fluidity of granules. The applied mechanical treatment did not alter the primary conformational properties of MOS except for destructing the intramolecular hydrogen bonds of cellulose and hemicellulose, thereby decreasing the crystallinity and thermal stability. Surface element analysis demonstrated more carbon-rich extractives on the particle surface as the particle size reduced. This study provided reasons behind improved dissolution and bioavailability of functional ingredients in plant-based granular materials by reducing particle size.

Keywords: crystallinity; cellulose; functional groups; hydrogen bonds

Introduction

Moringa oleifera Lam. belongs to the Moringaceae family with other names, including moringa, horseradish tree, and drumstick tree. This plant is commonly cultivated in many tropical and subtropical countries, such as India, Africa, Mexico, Southeast Asia, and southern Japan (Sugahara *et al.*, 2018). Various parts of the *M. Oleifera*, such as leaves, stems, roots, flowers, and seeds are rich in protein, dietary fiber, minerals, vitamins, and some bioactive compounds, and can be used as feed, herbal tea, nutritional supplements, food additives, and medicine for its dietary nutrition, functionality, and health benefits

(Gharibzahedi *et al.*, 2013; Yang *et al.*, 2020; Astrini *et al.*, 2020). Modern pharmacological research has revealed that *M. oleifera* possesses multiple nutraceutical or pharmacological activities, such as anti-inflammatory, antioxidant, anticancer, analgesic, hypoglycemic, and blood lipid-lowering functions due to the presence of multiple functional components, especially phenolic compounds, polysaccharides, and saponins (Sharma *et al.*, 2022; Zhou *et al.*, 2018).

A crucial step before using *Moringa oleifera* Lam. stem (MOS) is micronization using mechanical grinding. Many studies have shown that the reduced particle size

was beneficial to increasing the particle-specific surface area and cell wall breakage ratio, thereby accelerating the dissolution of bioactive ingredients and improving bioavailability and bioactivity *in vivo* or *in vitro* (Xiao *et al.*, 2017; Zhang & Zhai, 2020; Barreto *et al.*, 2021; Balakrishnan *et al.*, 2021; Qadri *et al.*, 2022). Huang *et al.* (2020) found that the decrease in particle size significantly reduced the water and oil holding capacities while increasing the lightness and yellowness of *M. oleifera* leaf powders. Sun *et al.* (2019) confirmed significantly improved flow properties, hydration properties, thermal stability, antioxidant activity, and cholesterol adsorption efficiency by reducing the particle size of black kidney bean powders. Sieve-based mechanical grinding, a traditional method to reduce the particle size of various materials, has been widely reported for various materials, including tobacco (Zhang *et al.*, 2022), green tea (Zaiter *et al.*, 2016), and black kidney bean (Sun *et al.*, 2019). Particle size significantly affects the physicochemical properties of granular materials. However, limited information is available on the particle size dependence of the physicochemical properties of MOS.

Therefore, this study's objective was to investigate the effect of particle size on the physicochemical properties of MOS, including color parameters, flow properties, hydration properties, thermal properties, and structural properties.

Materials and Methods

Sample preparation

Dried MOS was provided by Dehong Senbao Technology Development Co., Ltd. (Yunnan, China). After being cut into 2 cm segments, the samples were coarsely ground by a high-speed crusher (As One Co., Ltd., Shanghai, China) and sieved sequentially through a series of standard sieves with a pore size of 0.380, 0.250, 0.180, 0.120, 0.096, and 0.075 mm, corresponding to 40, 60, 80, 120, 160, and 200 mesh, respectively, using an electric vibrating screen machine (8411, Shangyu Daoxu xingfeng instrument factory, Zhejiang, China). The MOS powders between 40 and 60 mesh, 60 and 80 mesh, 80 and 120 mesh, 120 and 160 mesh, and 160 and 200 mesh were dominated as M40, M60, M80, M120, and M160, respectively. The MOS powders passed through a 200-mesh sieve were named M200.

Particle size

The particle size of powders was measured using a Mastersizer 3000 laser diffraction particle analyzer (Malvern instrument Ltd., Worcestershire, UK) using a dry test unit.

Particle parameters including D_{10} , D_{50} , D_{90} , specific surface area (A_{sf}), and span $[(D_{90}-D_{10})/D_{50}]$ were obtained. D_{10} , D_{50} , and D_{90} represented the 10%, 50%, and 90% cumulative percentiles of total volume, respectively. Span characterizes the particle size distribution width, and a larger value indicates a more inhomogeneous distribution.

Scanning electron microscopy (SEM)

A scanning electron microscope (SU8000, Hitachi Co., Tokyo, Japan) was applied to obtain the surface microstructure of MOS powders. Samples were spread onto the conductive adhesive tapes in a single layer, and gold particles were coated under a vacuum. An acceleration voltage of 10 kV and magnifications of $\times 50$ and $\times 300$ were used to obtain the SEM images.

Bulk density and tap density

Powders (5.0 g, M_1) were poured into a graduated cylinder with a total volume of 50 mL, and the volume occupied by the sample (V_1 , cm³) was read. Bulk density (ρ_{bulk} , g/cm³) can be calculated using Eq. (1). Tap density (ρ_{tap} , g/cm³) was determined using the modified Chinese National Standard methods (GB/T 21354-2008). The graduated cylinder with MOS powders was shaken on a thick sponge until an unchanged volume (V_2 , cm³). ρ_{tap} was calculated using Eq. (2).

$$\rho_{bulk} = \frac{M_1}{V_1} \quad (1)$$

$$\rho_{tap} = \frac{M_1}{V_2} \quad (2)$$

Angle of repose

The angle of repose (°) was tested following the modified method of Meng *et al.* (2017). A funnel was fixed vertically at 3 cm above the plane. The MOS powders were continuously poured into the funnel until the formed cone touched the funnel outlet. The angle of repose can be calculated as follows.

$$\text{Angle of repose} = \arctan \frac{H}{R} \quad (3)$$

where R (cm) and H (cm) were the radius and height of the formed cone, respectively.

Water and oil holding capacities

Water and oil holding capacities were determined using the modified method of Zhao *et al.* (2010). The MOS

powders (0.5 g, m_0) were poured into a centrifuge tube (m_1 , g), and 35 g of distilled water at 20°C was added. After storing in a refrigerator (4°C) for 24 h, the tubes were centrifuged at 11,180 × g for 10 min. The supernatant was discarded, and the total weight of the remaining sample and tube (m_2 , g) was recorded. Water holding capacity (WHC) can be calculated by Eq. (4).

$$WHC = \frac{m_2 - m_1 - m_0}{m_0} \quad (4)$$

The MOS powders (W_0 , 0.5 g) and corn oil (10 mL) were mixed in a plastic centrifuge tube (W_1 , g). The tubes were kept at room temperature for 1 h and then centrifuged at 11,180 × g for 15 min. The tubes with MOS powders (W_2 , g) were reweighted after gently discarding the supernatant. Oil holding capacity (OHC) was obtained using Eq. (5).

$$OHC = \frac{W_2 - W_1 - W_0}{W_0} \quad (5)$$

Color difference

Color parameters of MOS powders were quantitatively measured using a spectropolarimeter (Labscan XE, Hunterlab, USA). The CIE color parameter of L^* represents lightness, while a^* and b^* are greenness/redness and blueness/yellowness, respectively. The color difference (ΔE) can be calculated following Eq. (6).

$$\Delta E = \sqrt{(L^* - L_0)^2 + (a^* - a_0)^2 + (b^* - b_0)^2} \quad (6)$$

where L_0 , a_0 , and b_0 were the color parameters of the M40 sample, and L^* , a^* , and b^* were the color parameters of other MOS powders.

Fourier transform infrared (FTIR) spectroscopy

Samples were prepared using the pellet method by mixing potassium bromide (100 mg) and MOS powders (1 mg). An FTIR spectrometer (Nicolet iS5, Thermo Scientific, USA) was used for determination, and the spectrum was obtained over a wavenumber range of 4000-400 cm⁻¹ with 32 scans at a resolution of 4 cm⁻¹.

X-ray diffraction (XRD)

The XRD patterns of MOS powders with different particle sizes were measured by a wide-angle X-ray diffractometer (SmartLab, Rigaku, Japan) with Cu-Kα radiation (40 kV and 200 mA). Samples were loaded in a standard quartz sample holder and scanned from 5° to 45° (2θ) at 0.02° step size and 2°/min speed. The MDI Jade

6 software (Materials Data Inc, Livermore, CA) was applied to calculate the crystallinity index (CrI) by the peak area method (Toba *et al.*, 2013).

Thermogravimetric analysis (TGA)

TGA was carried out using a thermogravimetric analyzer (STA 449 F3 Jupiter, NETZSCH Instruments, Bavaria, Germany). Thermograms were recorded between 30 and 1000°C at a heating rate of 10°C/min and a 50 mL/min nitrogen flow rate. First derivatives of the thermograms (DTG), the weight loss percentage of each sample, and the related temperature parameters were analyzed using Universal Analysis Software (New Castle, Delaware, USA).

X-ray photoelectron spectroscopy (XPS)

The surface analysis of MOS powders was performed by an XPS system (ESCALAB Xi+, Thermo Fisher Scientific, UK) with a monochromatic Al Kα source (1486.6 eV, 14.4 kV, 13.6 mA) and a basic chamber pressure of 8 × 10⁻¹⁰ Pa. Each MOS sample was first analyzed with a survey scan using 100 eV pass energy at an energy step size of 1 eV. The pass energy of 30 eV's energy step size of 0.1 eV was used for data acquisition. The spot size was 500 μm, and the surface analysis depth was ~10 nm. The chemical-bond analysis of the carbon was performed by deconvoluting and fitting the C1s peak area region using Avantage software (Thermo Fisher Scientific Inc.). The oxygen to carbon (O/C) atomic ratio was estimated by the following Eq. (7) (Hua *et al.*, 1993).

$$O/C = I_o / 2.85 I_c \quad (7)$$

where I_o and I_c were the normalized integrated area of the O1s peak and C1s peak, respectively.

Statistical analysis

Data were presented as means of determinations ± standard deviation (n=3) and analyzed by SPSS 25.0 software (SPSS Inc., Chicago, IL, USA) to obtain the significance of the difference. Analysis of variance (ANOVA) with Duncan's multiple range test was applied, and a 0.95 confidence level ($P < 0.05$) was considered significant.

Results and Discussion

Particle size analysis

The particle size parameters are presented in Table 1. The particle size range of M40, M60, M80, M120, M160, and

Table 1. Particle size parameters of *Moringa oleifera* stem powders.

Samples	D_{10} (μm)	D_{50} (μm)	D_{90} (μm)	A_{sf} (m^2/kg)	Span
M40	214.7 \pm 0.9 ^e	458.3 \pm 1.2 ^f	1100.0 \pm 10.0 ^e	59.6 \pm 0.2 ^a	1.93 \pm 0.02 ^{ab}
M60	152.5 \pm 0.5 ^d	329.5 \pm 0.5 ^e	750.0 \pm 2.0 ^d	73.1 \pm 0.1 ^b	1.81 \pm 0.01 ^a
M80	77.8 \pm 1.1 ^c	230.0 \pm 1.0 ^d	600.5 \pm 6.5 ^c	92.6 \pm 1.1 ^c	2.27 \pm 0.04 ^{bc}
M120	24.8 \pm 1.3 ^b	139.7 \pm 2.4 ^c	337.3 \pm 28.3 ^b	130.0 \pm 1.6 ^d	2.23 \pm 0.06 ^{bc}
M160	10.6 \pm 0.3 ^a	53.7 \pm 1.5 ^b	126.0 \pm 2.0 ^a	346.6 \pm 3.9 ^e	2.16 \pm 0.10 ^{abc}
M200	8.0 \pm 0.1 ^a	36.3 \pm 0.9 ^a	105.7 \pm 10.8 ^a	526.8 \pm 2.2 ^f	2.46 \pm 0.07 ^c

Results were represented as mean values \pm standard deviation of triplicate tests. Different letters superscripted on the results were significantly different at $P < 0.05$.

M200 samples lay in 8.0–1100.0 μm , and their median particle size (D_{50}) was 458.3, 329.5, 230.0, 139.7, 53.7, and 36.3 μm , respectively, with significant differences between each other ($P < 0.05$). Generally, M40, M60, M80, and M120 samples belonged to tissue scale powders (500–100 μm), while M160 and M200 were cellular scales (50–30 μm) (Barakat *et al.*, 2015). These findings demonstrated that the plant scale could be reduced from organ to tissue and cell using sieve-based grinding. Fine powder (M200) owned a significantly ($P < 0.05$) higher span value than coarse powders (M40 and M60 samples). Similar observations were reported by He *et al.* (2019), who confirmed that more agglomerates appeared on the surface of ultrafine water dropwort powders. After grinding, the exposed polar groups may increase the electrostatic interaction of molecules, resulting in inhomogeneous powders and increasing span value (Xiao *et al.*, 2017). Moreover, with the decrease in particle size, the A_{sf} value significantly increased from 59.6 to 526.8 m^2/kg . Liu *et al.* (2019) and Zhang *et al.* (2021) also reported a similar correlation between particle size and A_{sf} . Decreasing particle size was accompanied by more particles per unit weight, owing a higher potential to achieve rapid dissolution and homogeneous mixing with the active pharmaceutical and food ingredients (Zhao *et al.*, 2010; Li *et al.*, 2020).

SEM micrographs

The SEM micrographs of MOS powders with different particle sizes are presented in Figure 1. Particle size was markedly decreased from M40 to M200. Strip-shaped structures were present in M40, M60, and M80 samples, and vascular bundles could be observed. The fiber structure was gradually destroyed by further reducing particle size and irregular shapes, especially strip and sheet structures. Granules were the smallest in the M200 sample, and original fiber structures were broken and destroyed entirely. It is worth noting that the porosity of the M200 sample was markedly reduced, and its particles had almost no internal pores. However, dimensional inhomogeneity was found in samples with smaller particle sizes

due to the agglomeration of small granules, which correlated well with the span values.

Bulk density and tap density

Density, a fundamental physical parameter of powdered materials, is crucial to the industrial processing of food powders. Density parameters can help manufacturers design packaging container volumes for powder products (Gao *et al.*, 2019). As shown in Table 2, the bulk and tap density decreased from 0.263 to 0.177 g/cm^3 and 0.303 to 0.206 g/cm^3 , respectively, as the particle size decreased from M40 to M160. The low density of tiny particles might be that the inter-particle forces were comparable with the particle mass, avoiding the powders forming dense structures (Liu *et al.*, 2017). However, the M200 sample owned higher bulk and tap density than M160, while still significantly lower than coarse MOS powders such as M40, M60, and M80. Decreasing intragranular closed pores and inter-particle voids in the M200 sample were responsible for this phenomenon (Meng *et al.*, 2017). Overall, cracks, hollows, closed pores in the particles, and the thin air film between the particles affected the density of the plant granules (Gao *et al.*, 2020).

Angle of repose

Angle of repose was used to characterize the fluidity of granular materials, and a smaller angle indicated the better flowability of granules. Table 2 presents the angle of repose of MOS powders. It was significantly ($P < 0.05$) reduced from 70.36° to 60.25° with decreasing particle size, demonstrating that the MOS particles became flowable. Similar results were also reported for *Quercus salicina* (Blume) leaf powders (Hong *et al.*, 2020) and hard white winter wheat (*Triticum aestivum* L.) bran powders (He *et al.*, 2018). Therefore, the fluidity of the MOS powders could be significantly improved by sieve-based mechanical grinding. However, Huang *et al.* (2020) found a significantly increased angle of repose for *M. oleifera*

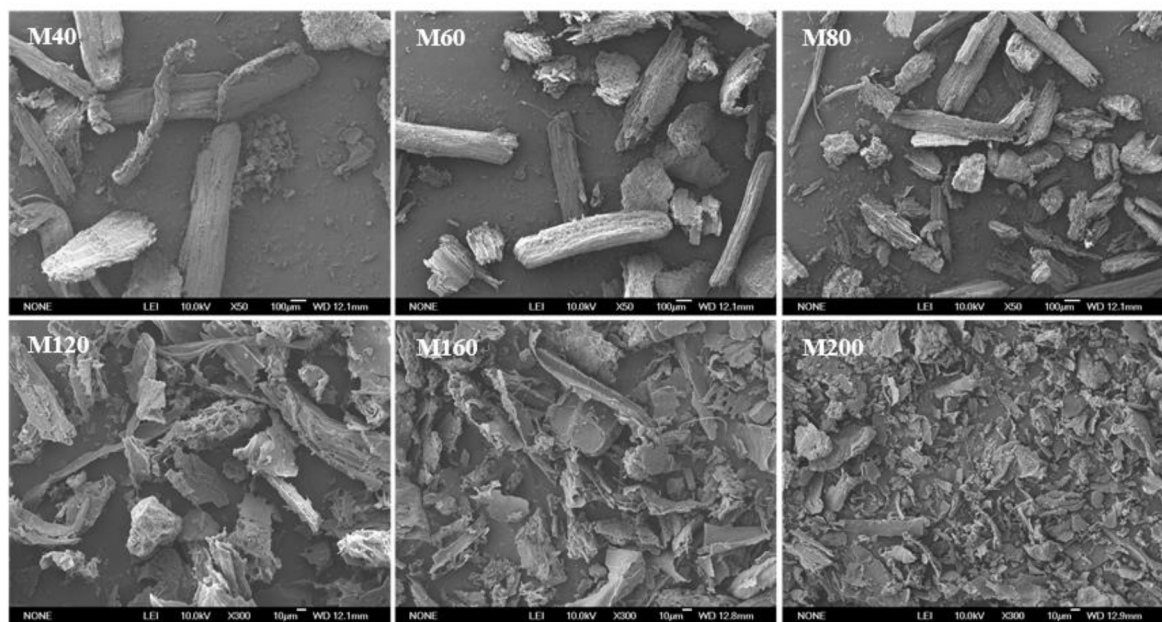


Figure 1. Scanning electron microscopy micrographs of *Moringa oleifera* stem powders with different particle sizes (M40, $\times 50$; M60, $\times 50$; M80, $\times 50$; M120, $\times 300$; M160, $\times 300$; M200, $\times 300$).

Table 2. Density, angle of repose, water and oil holding capacities, and color parameters of *Moringa oleifera* stem powders.

Samples	WHC (g/g)	OHC (g/g)	Bulk density (g/cm ³)	Tap density (g/cm ³)	Angle of repose (°)	L*	a*	b*	ΔE
M40	4.28 ± 0.02 ^a	3.02 ± 0.02 ^{ab}	0.263 ± 0.004 ^e	0.303 ± 0.005 ^d	70.36 ± 0.02 ^c	71.02 ± 0.17 ^b	1.58 ± 0.06 ^f	27.67 ± 0.10 ^d	0
M60	4.66 ± 0.12 ^{ab}	3.02 ± 0.04 ^{ab}	0.248 ± 0.002 ^d	0.297 ± 0.002 ^d	68.46 ± 0.71 ^{bc}	70.43 ± 0.16 ^a	1.32 ± 0.08 ^e	26.98 ± 0.08 ^c	0.96 ± 0.15 ^a
M80	4.88 ± 0.12 ^{ab}	3.44 ± 0.24 ^b	0.229 ± 0.003 ^c	0.285 ± 0.001 ^c	67.77 ± 0.43 ^b	70.31 ± 0.10 ^a	0.73 ± 0.02 ^d	27.50 ± 0.04 ^{cd}	1.12 ± 0.08 ^a
M120	5.69 ± 0.67 ^b	3.98 ± 0.01 ^c	0.182 ± 0.003 ^a	0.225 ± 0.003 ^b	66.29 ± 0.14 ^b	71.34 ± 0.18 ^b	0.26 ± 0.08 ^c	27.21 ± 0.20 ^{bc}	1.47 ± 0.16 ^b
M160	5.29 ± 0.13 ^{ab}	3.45 ± 0.17 ^b	0.177 ± 0.002 ^a	0.206 ± 0.002 ^a	62.12 ± 1.31 ^a	70.53 ± 0.04 ^a	-0.60 ± 0.01 ^b	26.02 ± 0.01 ^b	2.77 ± 0.01 ^c
M200	4.25 ± 0.47 ^a	2.71 ± 0.01 ^a	0.204 ± 0.004 ^b	0.225 ± 0.003 ^b	60.25 ± 0.36 ^a	70.45 ± 0.07 ^a	-0.99 ± 0.03 ^a	25.65 ± 0.09 ^a	3.31 ± 0.05 ^d

Results were represented as mean values \pm standard deviation of triplicate tests. Different letters superscripted on the results were significantly different at $P < 0.05$.

leaf powders as the particle size was reduced. This may be due to the different chemical compositions of *M. oleifera* leaf and stem. Finer *M. oleifera* leaf powders tended to agglomerate and arranged in a cone due to the significantly higher protein and fat contents than MOS (Zhao *et al.*, 2015b; Shih *et al.*, 2011).

Water and oil holding capacities

As shown in Table 2, the WHC values increased first with the decrease in particle size from M40 to M120 and then decreased from M120 to M200. As the particle size decreased, the increasing capillary attraction and material porosity and exposed hydrophilic groups in hemicellulose and cellulose improved the hydration

capacity of MOS (Meng *et al.*, 2017). However, polysaccharide chains, which could hold water by forming hydrogen bonds, may be destroyed in finer MOS powders, negatively affecting the hydration properties (Gao *et al.*, 2020). The OHC displayed a similar trend to WHC. The reduced particle size from M40 to M120 may also improve the capillarity absorption of the oil (He *et al.*, 2018). In contrast, fine particles, especially in the M200 sample, owned high bulk density, namely, smaller inter particulate spaces, reducing the capacity to hold interstitial water and oil (Zhao *et al.*, 2017). These results indicated that the decreasing particle size possessed the potential to integrate with water and absorb the dietary fat in the intestinal tract (Chen *et al.*, 2015; Zhong *et al.*, 2016), while the M200 sample negatively affected the functional properties of MOS.

Color analysis

Color is a crucial sensory parameter related to the consumer preference for food products developed from MOS. Color parameters of MOS powders with various particle sizes are listed in Table 2. Both a^* and b^* values significantly decreased as the particle size decreased, indicating that the powders turned to be greener and less yellow. The increase in the green spectrum may be related to the enhanced exposure to internal pigment compounds such as chlorophyll (He et al., 2019). Ramachandraiah and Chin (2016) found that decreasing particle size reduced persimmon peel in a^* and b^* values. Sun et al. (2019) also observed a decrease in b^* value as the particle size of black kidney bean powders decreased from 250–180 μm to 125–75 μm . Decreasing particle size increased ΔE dramatically, and a maximum value of 3.31 was found for the M200 sample compared to the M40 sample. Perceivable color difference is divided into three categories: very distinct ($\Delta E > 3$), distinct ($1.5 < \Delta E < 3$), and small difference ($\Delta E < 1.5$) (Adekunte et al., 2010). Based on these obtained results, sieve-based grinding displayed considerable influence on the color of MOS.

Functional group analysis

The FTIR is a useful tool for exploring organic materials' chemical composition and conformation by characterizing chemical bonds and functional groups (Xu et al., 2018). The FTIR spectra of MOS powders are illustrated in Figure 2. Various absorption peaks related to chemical constituents were observed. A broad band at 3500–3300 cm^{-1} represented the stretching vibration of O-H in polysaccharides and phenolic substances (He et al., 2019). The absorption peak at around 2920 cm^{-1} indicated stretching vibrations of C-H from proteins and polysaccharides

in MOS (Zhao et al., 2017). Three bands at approximately 1738, 1650, and 1510 cm^{-1} were attributed to carbonyl groups' bending or stretching vibrations (C=O), aromatic CH bonds, and C=C stretching bands, respectively (Zhao et al., 2015b; Ramachandraiah and Chin, 2016). The peaks centered at 1419 cm^{-1} and 1377 cm^{-1} indicated CH_2 and CH symmetric bending for cellulose and lignin, and the absorption at 1319 cm^{-1} suggested the C-N stretching vibration (Zhao et al., 2013). The peaks at around 1244 and 1030 cm^{-1} were ascribed to stretching vibration of C-O groups, corresponding to the pyranose ring from polysaccharides (Zhao et al., 2015b; He et al., 2019). With decreasing particle size, no new functional group was found. However, the accurate position of some chemical bands was altered to a higher wavenumber, suggesting that the sieve-based mechanical grinding did not alter the conformational properties of MOS except for the destruction of the intramolecular hydrogen bonds. Similar observations have been reported for persimmon by-products powders (Ramachandraiah and Chin, 2016) and red grape pomace powders (Zhao et al., 2015b). The hydrogen bond cleavage could enhance the material's external surface area and correspondingly improve the extraction yield of bioactive compounds (Hong et al., 2020).

XRD analysis

Figure 3 shows the XRD patterns of MOS powders with various particle sizes. Two crystalline peaks at around 16° and 22°, as well as a relatively weak peak at 35°, were observed, which were typical cellulose regions and corresponded to (101), (10 $\bar{1}$), (002), and (040) lattice planes of cellulose, respectively (Ji et al., 2016; Park et al., 2010). A broad peak appeared around 16° because the 101 and 10 $\bar{1}$ planes were close and overlapping (Zhao et al., 2017). As shown in Table 3, the CrI values were significantly ($P < 0.05$) reduced from 51.66% to 33.12% with decreasing

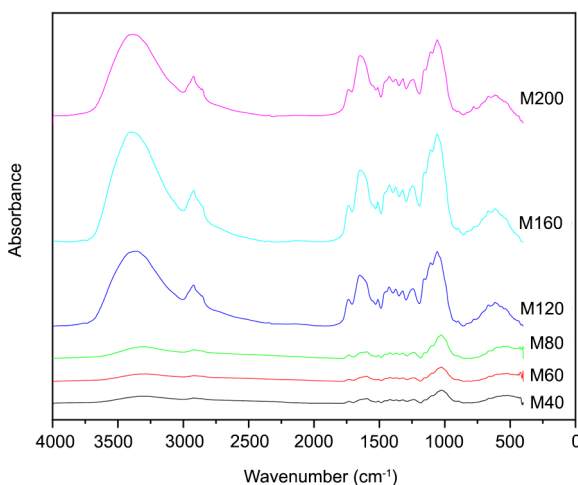


Figure 2. Fourier transform infrared spectra of *Moringa oleifera* stem powders with different particle sizes.

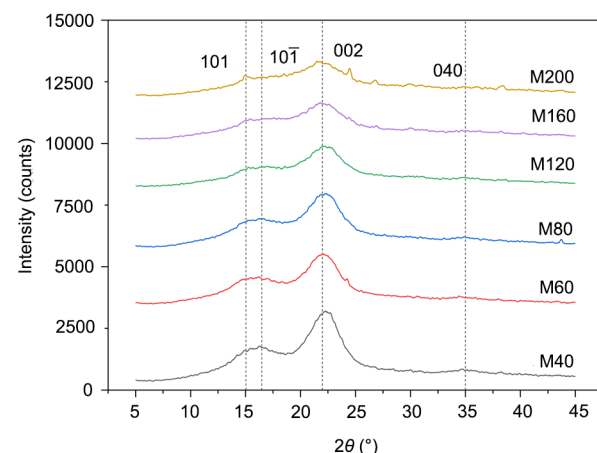


Figure 3. X-ray diffraction patterns of *Moringa oleifera* stem powders with different particle sizes.

Table 3. Weight loss due to water desorption (WL), temperature values corresponding to the onset of the decomposition process (T_{ei}) and the maximum degradation rate (T_{deg}), and crystallinity index (CrI) of *Moringa oleifera* stem powders.

Samples	WL (wt%)	T_{ei} (°C)	T_{deg} (°C)	Maximum deriv. weight (wt%/°C)	CrI (%)
M40	2.89 ± 0.00 ^{ab}	278.40 ± 1.41 ^{dc}	324.62 ± 0.40 ^{dc}	0.94 ± 0.02 ^{dc}	51.66 ± 2.48 ^d
M60	2.68 ± 0.21 ^a	276.16 ± 0.69 ^d	323.83 ± 0.10 ^d	0.87 ± 0.04 ^c	47.87 ± 0.30 ^c
M80	2.78 ± 0.00 ^a	277.67 ± 0.55 ^{db}	323.79 ± 0.41 ^{db}	0.89 ± 0.01 ^{cd^b}	45.25 ± 1.11 ^{bc}
M120	2.86 ± 0.03 ^{ab}	272.68 ± 1.05 ^c	322.62 ± 0.05 ^{cb}	0.85 ± 0.01 ^c	42.73 ± 1.31 ^b
M160	3.07 ± 0.04 ^{bc}	265.96 ± 1.29 ^{ba}	320.55 ± 0.65 ^{ba}	0.74 ± 0.03 ^{ba}	35.90 ± 0.49 ^a
M200	3.14 ± 0.10 ^c	262.28 ± 1.31 ^a	319.59 ± 0.00 ^a	0.66 ± 0.00 ^a	33.12 ± 0.90 ^a

Results were represented as mean values ± standard deviation of triplicate tests. Different letters superscripted on the results were significantly different at $P < 0.05$.

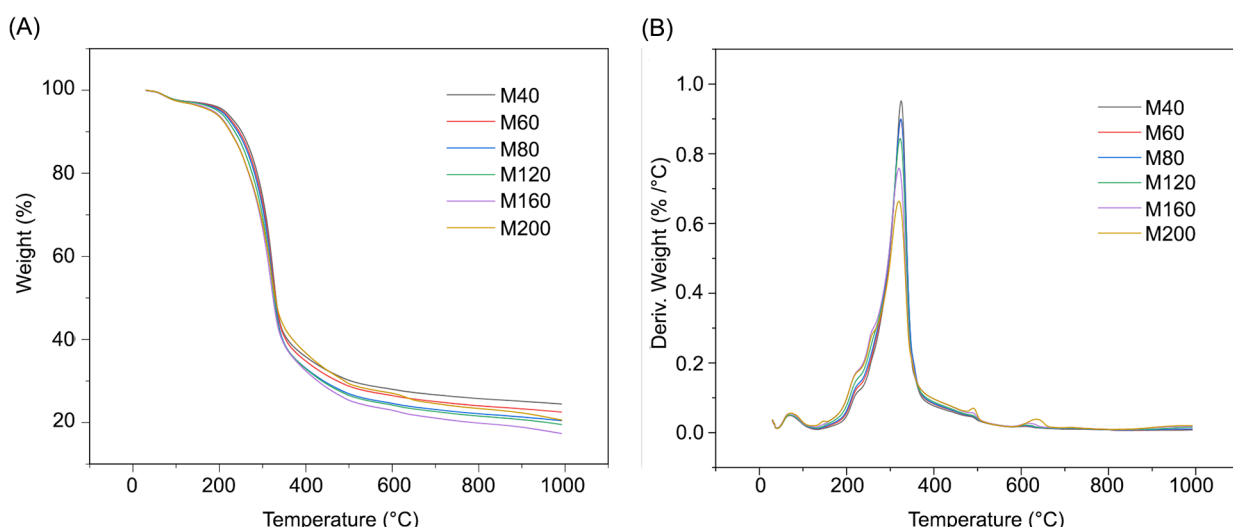


Figure 4. Thermogravimetry (A) and derivative thermogravimetry (B) curves of *Moringa oleifera* stem powders with different particle sizes.

particle size. The ordered structure of cellulose was destroyed, and other studies have also reported a similar tendency (Yang *et al.*, 2014). Combined with FTIR findings, a fact can be generalized that the applied mechanical force disrupted the hydrogen bonds associated with the crystal structure of cellulose and hemicellulose, and new amorphous cellulose and soluble saccharides might be formed. However, some opposed results were reported that the reduced particle size increased the CrI values of corn stalk (Zhao *et al.*, 2013), tobacco (Zhang *et al.*, 2022), ginger (Zhao *et al.*, 2015a), *Dendrobium officinale* (Meng *et al.*, 2018), and *M. oleifera* leaf powders (Huang *et al.*, 2020) because amorphous cellulose was more reactive. Some new crystals were reconstructed during processing (Zhao *et al.*, 2013).

Thermal analysis

The thermal properties of the MOS powders with different particle sizes are displayed in Figure 4. The TGA (Figure 4A)

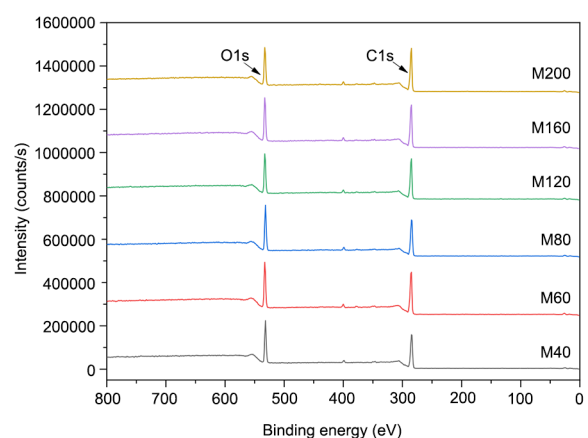


Figure 5. X-ray photoelectron spectra of the O1s and C1s peaks for *Moringa oleifera* stem powders with different particle sizes.

and DTG (Figure 4B) curves were analyzed to study the thermal behaviors of the MOS powders. Weight loss of material occurred at three different temperature regions.

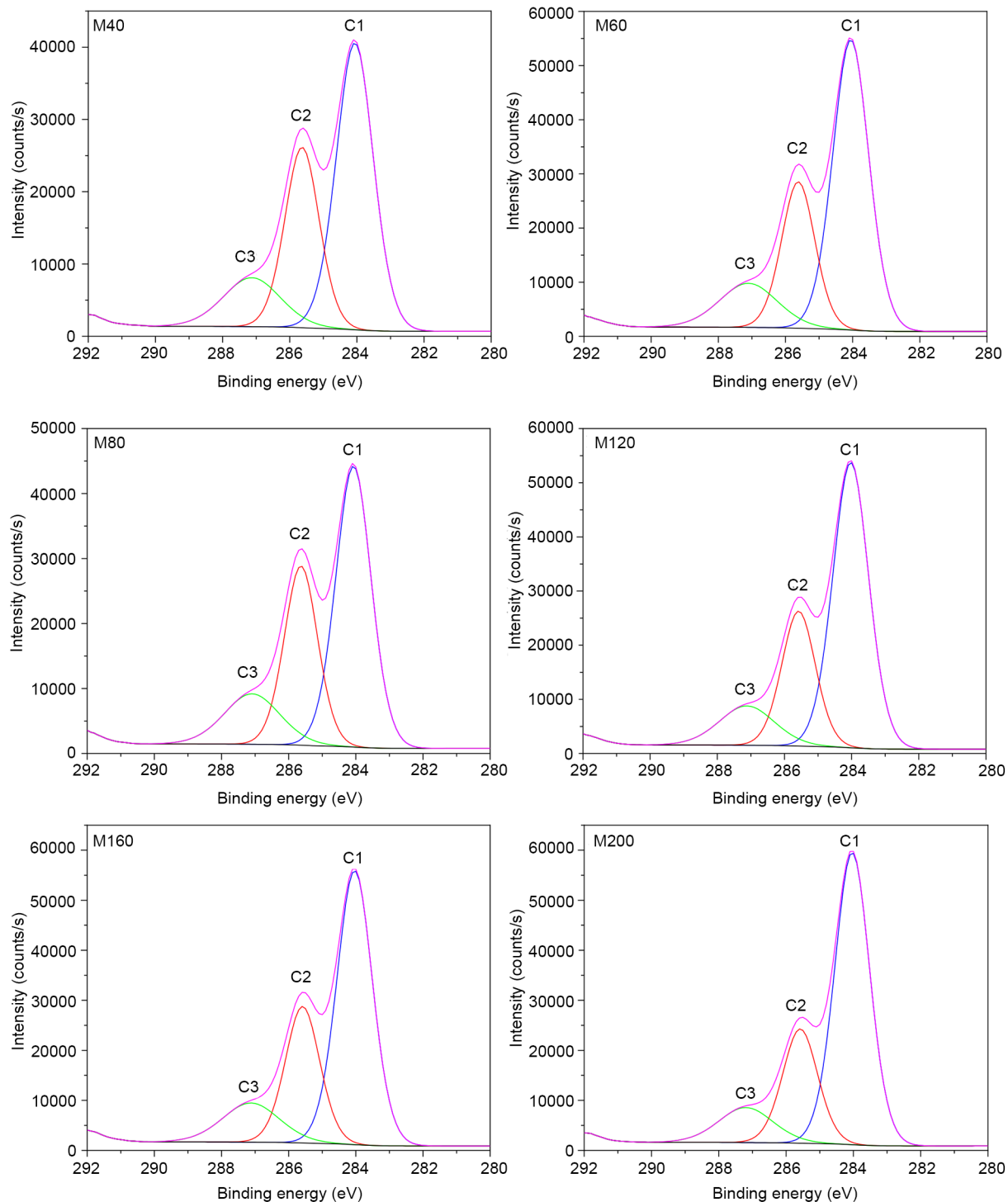


Figure 6. Deconvoluted C1s peak area region for *Moringa oleifera* stem powders with different particle sizes.

In the first stage, around 3% of the initial weight of the MOS powders was lost as the temperature ranged from 30 to 200°C. This was probably due to the evaporation of adsorbed and structural water and light volatiles (Meng

et al., 2018). At a temperature of 200–500°C (the second stage), the powders lost most of their initial weight because many organic substances, including hemicellulose, cellulose, and lignin, were decomposed (Chen

and Kuo, 2010). When the temperature was higher than 500°C (the third stage), thermal decomposition of other heavy components occurred, while the weight loss was not very distinct. Carbonized residues were finally retained, which accounted for about 17%-25% of the initial mass.

Percentage weight loss due to water desorption (WL) and temperature values corresponding to the onset of the decomposition process (T_{ei}) and the maximum degradation rate (T_{deg}) are summarized in Table 3. It can be found from the first weight-loss stage that the WL increased with the decrease in particle size. This phenomenon was related to crystal structure and the affinity of the water to the powder. Increasing amorphous fraction in finer powders would absorb more water molecules, while crystalline domains were less accessible to water (Avolio *et al.*, 2012). In the second stage, the samples with smaller particle sizes possessed lower T_{ei} value, T_{deg} value, and maximum derivative weights. This is owing to the higher content of amorphous cellulose, which could be degraded without overcoming the energy barrier of the crystal structure (Wang *et al.*, 2013). These results demonstrated that sieve-based grinding could destroy the crystal structure of cellulose and form amorphous domains, reducing the thermal stability of MOS powders. These observations correlated well with the FTIR and XRD results.

XPS analysis

XPS characterized the surface composition of MOS powders, and the O1s peak and C1s peak were found to be present in noticeable amounts (Figure 5). According to the classification of carbon atoms in plant-based materials, the C1s peak can be deconvoluted into four subpeaks at

approximately 284.8 eV (C1) and 286.3 eV (C2), 287.8 eV (C3), and 289.0 eV (C4). C1 corresponds to C–C/C–H, mainly from lignin and extractives; C2 corresponds to C–O, mainly from cellulose and hemicellulose; C3 corresponds to C=O/O–C–O; and C4 corresponds to O–C=O (Sinn *et al.*, 2001). The C1s spectra of MOS powders with different particle sizes were deconvoluted into three Gaussian peaks, including C1, C2, and C3 (Figure 6). At the same time, C4 was not found in the XPS spectra, indicating an undetectable concentration of O=C–O groups in MOS samples, as seen elsewhere (Yang *et al.*, 2014). The theoretical O/C ratios of cellulose, hemicellulose, lignin, and extractives were 0.83, 0.8, 0.33, and 0.11, respectively (Ji *et al.*, 2016; Kocaeef *et al.*, 2013). With the decrease in particle size, the O/C atomic ratio and the area percentages of C2 peak and C3 peak decreased, while the area percentage of C1 peak increased (Table 4). The increasing C1 component and decreasing O/C ratio indicated more carbon-rich extractives, including fats, terpenes, and lignin guaiacyl units on the surface of MOS powders (Kocaeef *et al.*, 2013). Therefore, the present study results demonstrated that the reduced particle size improved the exposure, dissolution, extraction, and bioaccessibility of bioactive ingredients in plant-based granular materials.

Conclusions

Moringa oleifera Lam. stem powders with median particle sizes ranging from 458.3 to 36.3 µm were produced using sieve-based grinding. The microstructure showed that the fiber was gradually destroyed, and irregular strip- and sheet-shaped structures were observed with decreasing particle size. The decreasing particle size reduced density and angle of repose while increasing water and oil capacities. However, the smallest particle size of 36.3 µm reduced hydration properties and increased powder density due to reduced porosity. Regarding the color, decreasing particle size increased greenness and reduced yellowness. After grinding, no new functional group was found in Fourier transform infrared spectra, but the accurate position was shifted to a higher wavenumber. The decreasing particle size reduced the crystallinity index (from 51.66% to 33.12%) and the thermal stability of powders (e.g., maximum degradation temperature from 324.62 to 319.59°C). The above structural analysis demonstrated the destroyed hydrogen bonds associated with cellulose and hemicellulose crystal structure. The decreasing surface O/C ratio of powder with decreasing particle size indicated more carbon-rich extractives on the powder surface. Future studies must investigate the dissolution and bioavailability of active compounds in *M. oleifera* Lam. stem powders.

Table 4. Area percentage of C1-C3 peaks by deconvoluting C1s peak region and surface O/C atomic ratio of *Moringa oleifera* stem powders with different particle sizes.

Samples	C1 (%)	C2 (%)	C3 (%)	O/C
M40	55.42 ± 1.73 ^a	30.27 ± 1.81 ^a	14.31 ± 0.08 ^c	0.35 ± 0.01 ^b
M60	59.52 ± 1.44 ^a	26.68 ± 0.80 ^a	13.80 ± 0.64 ^{bc}	0.32 ± 0.01 ^{ab}
M80	57.56 ± 6.30 ^a	28.13 ± 5.33 ^a	14.31 ± 0.97 ^c	0.32 ± 0.04 ^{ab}
M120	60.23 ± 0.23 ^a	26.85 ± 0.05 ^a	12.92 ± 0.18 ^{ab}	0.30 ± 0.01 ^{ab}
M160	59.01 ± 0.89 ^a	27.70 ± 0.73 ^a	13.29 ± 0.16 ^{bc}	0.31 ± 0.00 ^{ab}
M200	62.59 ± 1.03 ^a	25.59 ± 1.03 ^a	11.83 ± 0.01 ^a	0.29 ± 0.01 ^a

Results were represented as mean values ± standard deviation of triplicate tests. Different letters superscripted on the results were significantly different at $P < 0.05$.

References

- Adekunte, A.O., Tiwari, B.K., Cullen, P.J., Scannell, A.G.M. and O' Donnell, C.P., 2010. Effect of sonication on colour, ascorbic acid and yeast inactivation in tomato juice. *Food Chemistry* 122: 500–507. <https://doi.org/10.1016/j.foodchem.2010.01.026>
- Astrini, N.J., Rakhamwati, T., Sumadi, S. and Bakti, I.G.M.Y., 2020. Identifying objective quality attributes of functional foods. *Quality Assurance and Safety of Crops & Foods* 12(2): 24–39
- Avolio, R., Bonadies, I., Capitani, D., Errico, M.E., Gentile, G. and Avella, M., 2012. A multi-technique approach to assess the effect of ball milling on cellulose. *Carbohydrate Polymer* 87: 265–273. <https://doi.org/10.1016/j.carbpol.2011.07.047>
- Balakrishnan, M., Gayathiri, S., Preetha, P., Pandiselvam, R., Jeevarathinam, G., Delfiya, D.A. and Kothakota, A., 2021. Micro-encapsulation of bixin pigment by spray drying: evaluation of characteristics. *Lebensmittel-Wissenschaft & Technologie* 145: 111343.
- Barakat, A., Monlau, F., Solhy, A. and Carrere, H., 2015. Mechanical dissociation and fragmentation of lignocellulosic biomass: effect of initial moisture, biochemical and structural properties on energy requirement. *Applied Energy* 142: 240–246. <https://doi.org/10.1016/j.apenergy.2014.12.076>
- Barretto, R., Buenavista, R.M., Pandiselvam, R. and Siliveru, K., 2021. Influence of milling methods on the flow properties of ivory teff flour. *Journal of Texture Studies*. Preprint. <https://doi.org/10.1111/jtxs.12630>
- Chen, W. and Kuo, P., 2010. A study on torrefaction of various biomass materials and its impact on lignocellulosic structure simulated by a thermogravimetry. *Energy* 35: 2580–2586. <https://doi.org/10.1016/j.energy.2010.02.054>
- Chen, Y., Zhang, B., Sun, Y., Zhang, J., Sun, H. and Wei, Z., 2015. Physicochemical properties and adsorption of cholesterol by okra (*Abelmoschus esculentus*) powder. *Food & Function* 6: 3728–3736. <https://doi.org/10.1039/c5fo00600g>
- Gao, W., Chen, F., Wang, X. and Meng, Q., 2020. Recent advances in processing food powders by using superfine grinding techniques: a review. *Comprehensive Reviews in Food Science and Food Safety* 19: 2222–2255. <https://doi.org/10.1111/1541-4337.12580>
- Gao, X., Zhu, D., Liu, Y., Zha, L., Chen, D. and Guo, H., 2019. Physicochemical properties and anthocyanin bioaccessibility of downy rose-myrtle powder prepared by superfine grinding. *International Journal of Food Properties* 22: 2022–2032. <https://doi.org/10.1080/10942912.2019.1702999>
- Gharibzahedi, S.M.T., Ansarifard, I., Hasanabadi, Y.S., Ghahderijani, M. and Yousefi, R., 2013. Physicochemical properties of *Moringa peregrina* seed and its oil. *Quality Assurance and Safety of Crops & Foods* 5(4): 303–309. <https://doi.org/10.3920/QAS2012.0172>
- He, S., Li, J., He, Q., Jian, H., Zhang, Y., Wang, J. and Sun, H., 2018. Physicochemical and antioxidant properties of hard white winter wheat (*Triticum aestivum* L.) bran superfine powder produced by eccentric vibratory milling. *Powder Technology* 325: 126–133. <https://doi.org/10.1016/j.powtec.2017.10.054>
- He, S., Tang, M., Sun, H., Ye, Y., Cao, X. and Wang, J., 2019. Potential of water dropwort (*Oenanthe javanica* DC.) powder as an ingredient in beverage: functional, thermal, dissolution and dispersion properties after superfine grinding. *Powder Technology* 353: 516–525. <https://doi.org/10.1016/j.powtec.2019.05.048>
- Hong, S.J., Das, P.R. and Eun, J.B., 2020. Effects of superfine grinding using ball-milling on the physical properties, chemical composition, and antioxidant properties of *Quercus salicina* (Blume) leaf powders. *Journal of the Science of Food and Agriculture* 101: 3123–3131. <https://doi.org/10.1002/jsfa.10941>
- Hua, X., Kaliaguine, S., Kokta, B. and Adnot, A., 1993. Surface analysis of different wood. *Wood Science and Technology* 27: 449–459.
- Huang, X., Liang, K., Liu, Q., Qiu, J., Wang, J. and Zhu, H., 2020. Superfine grinding affects physicochemical, thermal and structural properties of *Moringa Oleifera* leaf powders. *Industrial Crops and Products* 151: 112472. <https://doi.org/10.1016/j.indcrop.2020.112472>
- Ji, G., Gao, C., Xiao, W. and Han, L., 2016. Mechanical fragmentation of corncob at different plant scales: impact and mechanism on micro-structure features and enzymatic hydrolysis. *Bioresource Technology* 205: 159–165. <https://doi.org/10.1016/j.biortech.2016.01.029>
- Kocaefe, D., Huang, X., Kocaefe, Y. and Boluk, Y., 2013. Quantitative characterization of chemical degradation of heat-treated wood surfaces during artificial weathering using XPS. *Surface and Interface Analysis* 45: 639–649. <https://doi.org/10.1002/sia.5104>
- Li, G., Guo, W., Gao, X., Wang, Y. and Sun, S., 2020. Effect of superfine grinding on physicochemical and antioxidant properties of soybean residue powder. *Food Science & Nutrition* 8: 1208–1214. <https://doi.org/10.1002/fsn3.1409>
- Liu, H., Chen, X., Ji, G., Yu, H., Gao, C., Han, L. and Xiao, W., 2019. Mechanochemical deconstruction of lignocellulosic cell wall polymers with ball-milling. *Bioresource Technology* 286: 121364. <https://doi.org/10.1016/j.biortech.2019.121364>
- Liu, Y., Lu, H., Poletto, M., Guo, X. and Gong, X., 2017. Bulk flow properties of pulverized coal systems and the relationship between inter-particle forces and particle contacts. *Powder Technology* 322: 226–240. <https://doi.org/10.1016/j.powtec.2017.07.057>
- Meng, Q., Fan, H., Chen, F., Xiao, T. and Zhang, L., 2018. Preparation and characterization of *Dendrobium officinale* powders through superfine grinding. *Journal of the Science of Food and Agriculture* 98: 1906–1913. <https://doi.org/10.1002/jsfa.8672>
- Meng, Q., Fan, H., Xu, D., Aboshora, W., Tang, Y., Xiao, T. and Zhang, L., 2017. Superfine grinding improves the bioaccessibility and antioxidant properties of *Dendrobium officinale* powders. *International Journal of Food Science & Technology* 52: 1440–1451. <https://doi.org/10.1111/ijfs.13405>
- National Standards of People's Republic of China. 2016. Powders-determination of tap density, GB/T 21354-22008, Beijing.
- Park, S., Baker, J.O., Himmel, M.E., Parilla, P.A. and Johnson, D.K., 2010. Cellulose crystallinity index: measurement techniques and their impact on interpreting cellulase performance. *Biotechnology for Biofuels* 3: 10. <https://doi.org/10.1186/1754-6834-3-10>
- Qadri, T., Naik, H.R., Hussain, S.Z., Ahad, T., Shafi, F. and Sharma, M.K., 2022. Comparative evaluation of apple juice concentrate and spray dried apple powder for nutritional, antioxidant and rheological behaviour. *Quality Assurance and Safety of Crops & Foods* 14(2): 74–85.
- Ramachandraiah, K. and Chin, K.B., 2016. Evaluation of ball-milling time on the physicochemical and antioxidant properties of

- persimmon by-products powder. Innovative Food Science & Emerging Technologies 37: 115–124. <https://doi.org/10.1016/j.ifset.2016.08.005>
- Sharma, K., Kumar, M., Waghmare, R., Suhag, R., Gupta, O.P., Lorenzo, J.M., Prakash, S., Radha, Rais, N., Sampathraj, V., Thappa, C., Anitha, T., Sayed, A.A.S., Abdel-Wahab, B.A., Senapathy, M., Pandiselvam, R., Dey, A., Dhumal, S., Amarowicz, R. and Kennedy, J.E., 2022. *Moringa (Moringa oleifera Lam.) polysaccharides: extraction, characterization, bioactivities, and industrial application.* International Journal of Biological Macromolecules 209: 763–778. <https://doi.org/10.1016/j.ijbiomac.2022.04.047>
- Shih, M., Chang, C., Kang, S. and Tsai, M., 2011. Effect of different parts (leaf, stem and stalk) and seasons (summer and winter) on the chemical compositions and antioxidant activity of *Moringa oleifera*. International Journal of Molecular Sciences 12: 6077–6088. <https://doi.org/10.3390/ijms12096077>
- Sinn, G., Reiterer, A. and Stanzl-Tschegg, S.E., 2001. Surface analysis of different wood species using X-ray photoelectron spectroscopy (XPS). Journal of Materials Science 36: 4673–4680. <https://doi.org/10.1023/A:1017954300015>
- Sugahara, S., Chiyo, A., Fukuoka, K., Ueda, Y., Tokunaga, Y., Nishida, Y., Kinoshita, H., Matsuda, Y., Igoshi, K., Ono, M. and Yasuda, S., 2018. Unique antioxidant effects of herbal leaf tea and stem tea from *Moringa oleifera* L. especially on superoxide anion radical generation systems. Bioscience, Biotechnology, and Biochemistry 82: 1973–1984. <https://doi.org/10.1080/09168451.2018.1495552>
- Sun, X., Zhang, Y., Li, J., Aslam, N., Sun, H., Zhao, J., Wu, Z. and He, S., 2019. Effects of particle size on physicochemical and functional properties of superfine black kidney bean (*Phaseolus vulgaris* L.) powder. PEERJ 7: e6369. <https://doi.org/10.7717/peerj.6369>
- Toba, K., Yamamoto, H. and Yoshida, M., 2013. Crystallization of cellulose microfibrils in wood cell wall by repeated dry-and-wet treatment, using X-ray diffraction technique. Cellulose 20: 633–643. <https://doi.org/10.1007/s10570-012-9853-7>
- Wang, Z., McDonald, A.G., Westerhof, R.J.M., Kersten, S.R.A., Cuba-Torres, C.M., Ha, S., Pecha, B. and Garcia-Perez, M., 2013. Effect of cellulose crystallinity on the formation of a liquid intermediate and on product distribution during pyrolysis. Journal of Analytical and Applied Pyrolysis 100: 56–66. <https://doi.org/10.1016/j.jaat.2012.11.017>
- Xiao, W., Zhang, Y., Fan, C. and Han, L., 2017. A method for producing superfine black tea powder with enhanced infusion and dispersion property. Food Chemistry 214: 242–247. <https://doi.org/10.1016/j.foodchem.2016.07.096>
- Xu, Y., Hassan, M.M., Kutsanadzie, F.Y.H., Li, H.H. and Chen, Q.S., 2018. Evaluation of extra-virgin olive oil adulteration using FTIR spectroscopy combined with multivariate algorithms. Quality Assurance and Safety of Crops & Foods 10(4): 411–421. <https://doi.org/10.3920/QAS2018.1330>
- Yang, S.L., Yang, R.C., Zhou, X., Yang, S.H., Luo, L.L., Zhu, Y.C. and Boonanuntan, S., 2020. Effects of feeding diets with processed *Moringa oleifera* stem meal on growth and laying performance, and immunological and antioxidant activities in laying ducks. Poultry Science 99: 3445–3451. <https://doi.org/10.1016/j.psj.2020.04.002>
- Yang, Y., Ji, G., Xiao, W. and Han, L., 2014. Changes to the physico-chemical characteristics of wheat straw by mechanical ultrafine grinding. Cellulose, 21: 3257–3268. <https://doi.org/10.1007/s10570-014-0381-5>
- Zaiter, A., Becker, L., Karam, M. and Dicko, A., 2016. Effect of particle size on antioxidant activity and catechin content of green tea powders. Journal of Food Science and Technology 53: 2025–2032. <https://doi.org/10.1007/s13197-016-2201-4>
- Zhang, Y., Li, R., Shang, G., Zhu, H., Mahmood, N. and Liu, Y., 2021. Mechanical grinding alters physicochemical, structural, and functional properties of tobacco (*Nicotiana tabacum* L.) leaf powders. Industrial Crops and Products 173: 114149. <https://doi.org/10.1016/j.indcrop.2021.114149>
- Zhang, Y., Li, R., Shang, G., Zhu, H., Wang, H., Pandiselvam, R., Lei, D., Ai, Z. and Liu, Y., 2022. Effects of multiscale-mechanical fragmentation on techno-functional properties of industrial tobacco waste. Powder Technology 402: 117327. <https://doi.org/10.1016/j.powtec.2022.117327>
- Zhang, J. and Zhai, A., 2020. Microstructure, thermodynamics, and rheological properties of different types of red adzuki bean starch. Quality Assurance and Safety of Crops & Foods 12(2): 89–99.
- Zhao, D., Yang, F., Dai, Y., Tao, F., Shen, Y., Duan, W., Zhou, X., Ma, H., Tang, L. and Li, J., 2017. Exploring crystalline structural variations of cellulose during pulp beating of tobacco stems. Carbohydrate Polymer 174: 146–153. <https://doi.org/10.1016/j.carbpol.2017.06.060>
- Zhao, X., Chen, J., Chen, F., Wang, X., Zhu, Q. and Ao, Q., 2013. Surface characterization of corn stalk superfine powder studied by FTIR and XRD. Colloids and Surfaces B: Biointerfaces 104: 207–212. <https://doi.org/10.1016/j.colsurfb.2012.12.003>
- Zhao, X., Du, F., Zhu, Q., Qiu, D., Yin, W. and Ao, Q., 2010. Effect of superfine pulverization on properties of Astragalus membranaceus powder. Powder Technology 203: 620–625. <https://doi.org/10.1016/j.powtec.2010.06.029>
- Zhao, X., Zhu, H., Chen, J. & Ao, Q., 2015a. FTIR, XRD and SEM analysis of ginger powders with different size. Journal of Food Processing and Preservation 39: 2017–2026. <https://doi.org/10.1111/jfpp.12442>
- Zhao, X., Zhu, H., Zhang, G. and Tang, W., 2015b. Effect of superfine grinding on the physicochemical properties and antioxidant activity of red grape pomace powders. Powder Technology 286: 838–844. <https://doi.org/10.1016/j.powtec.2015.09.025>
- Zhao, Y., Wu, X., Wang, Y., Jing, R. and Yue, F., 2017. Comparing physicochemical properties of hawthorn superfine and fine powders. Journal of Food Processing & Preservation 41: e12834. <https://doi.org/10.1111/jfpp.12834>
- Zhong, C., Zu, Y., Zhao, X., Li, Y., Ge, Y., Wu, W., Zhang, Y., Li, Y. and Guo, D., 2016. Effect of superfine grinding on physico-chemical and antioxidant properties of pomegranate peel. International Journal of Food Science & Technology 51: 212–221. <https://doi.org/10.1111/ijfs.12982>
- Zhou, Y., Yang, W., Li, Z., Luo, D., Li, W., Zhang, Y., Wang, X., Fang, M., Chen, Q. and Jin, X., 2018. *Moringa oleifera* stem extract protect skin keratinocytes against oxidative stress injury by enhancement of antioxidant defense systems and activation of PPAR α . Biomedicine & Pharmacotherapy 107: 44–53. <https://doi.org/10.1016/j.biopha.2018.07.152>